

Magnetic Fields and Ionized Gas in the inner Galaxy: An Outer Scale for Turbulence and the Possible Role of H II Regions

M. Haverkorn¹, B. M. Gaensler¹, N. M. McClure-Griffiths^{2,3}, John M. Dickey⁴, and A. J. Green⁵

ABSTRACT

We present an analysis of rotation measure (RM) fluctuations from the Test Region of the Southern Galactic Plane Survey (SGPS), along with emission measure (EM) fluctuations in the same field taken from the Southern H-Alpha Sky Survey Atlas. The structure function of RM fluctuations shows a relatively steep slope at small scales (1 – 5 arcmin), a break in slope to a flatter structure function at intermediate scales (5 – 60 arcmin), and a systematic variation of the strength of fluctuations as a function of position angle on the sky at the largest scales (60 – 200 arcmin). The structure function of EM fluctuations shows similar behavior, although the lower resolution of the data prevents detection of a possible break in the spectrum. We interpret the anisotropy in RM/EM structure on large scales as resulting from a large-scale gradient in electron density (and possibly magnetic field) across the region. The break in the slope of the RM structure function at scales of ~ 5 arcmin can be explained by contributions from two spatially distinct magneto-ionized screens, most likely in the Local and Carina spiral arms. The observed structure function then implies that the outer scale of RM fluctuations in these screens is ~ 2 pc. Such behavior is in striking contrast to the expectation that interstellar turbulence forms an unbroken spectrum from kpc down to AU scales. We conclude that we have identified an additional source of enhanced turbulence, injected on scales of a few pc, possibly seen only in the Galactic plane. The most likely source of such turbulence is individual H II regions from relatively low-mass stars, whose characteristic scale size is similar to the outer scale of turbulence inferred here. These sources may be the dominant source of density and velocity fluctuations in warm ionized gas in the Galactic plane.

Subject headings: Galaxy: structure — H II regions — ISM: structure — techniques: polarimetric — radio continuum: ISM — turbulence

1. INTRODUCTION

The evidence for the presence of turbulence in the interstellar medium (ISM) is overwhelming. Although some studies of the characteristics of this turbulence (viz. the inner and outer scales, shape of the spectrum and power law spectral index) indicate the presence of standard incompressible Kolmogorov (1941) turbulence, many observations indicate different kinds of turbulence, drivers and environments. Armstrong, Rickett & Spangler (1995) compiled observations of (among others) interstellar scattering of pulsars and extragalactic sources, dispersion measures of pulsars and rotation measures (RM) of extragalactic sources in one

¹Harvard-Smithsonian Center for Astrophysics, 60 Garden Street, Cambridge MA 01238; mhaverkorn@cfa.harvard.edu, bgaensler@cfa.harvard.edu

²Australia Telescope National Facility, CSIRO, P.O. Box 76, Epping, NSW 1710, Australia; naomi.mcclure-griffiths@csiro.au

³Bolton Fellow

⁴Department of Astronomy, University of Minnesota, 116 Church Street, SE, Minneapolis, MN 55455; john@astro.umn.edu

⁵School of Physics, University of Sydney, NSW 2006, Australia; agreeen@physics.usyd.edu.au

power spectrum. The result was the so-called “big power law in the sky”, a Kolmogorov-like power spectrum of electron density fluctuations over 12 orders of magnitude, from a fraction of an AU to kiloparsecs. Although the big power law in the sky is very well-determined on small scales (up to ~ 0.001 pc), the extension towards larger scales is based only on two types of measurements: the RM of extragalactic sources, which gives an upper limit to the amount of structure in the electron density because the contribution of the magnetic field is unknown; and from velocity measurements of H I, making assumptions about the connection between neutral and ionized material.

The dominant source for the large-scale energy input in the Galaxy is generally assumed to be supernova explosions (Spitzer 1978; Vollmer & Beckert 2002; Korpi et al. 1999). Other possible sources are superbubbles, massive H II regions and massive stellar winds (Norman & Ferrara 1996), Galactic fountains, chimneys, or gravitational scattering by transient spiral waves (see Sellwood & Balbus (1999) and references therein), gravitational instabilities in a shearing disk (Elmegreen, Elmegreen & Leitner 2003), or magneto-rotational instabilities (Mac Low & Klessen 2004). The big power law in the sky certainly suggests the classical scenario of turbulent energy input on large scales, which cascades down to smaller scales until the energy is dissipated on the smallest scale (Kolmogorov 1941).

However, there are indications of other types of turbulence in the ISM as well. Minter & Spangler (1996) found a break in the structure function of RMs of extragalactic sources and emission measures (EM) of the warm ionized gas on scales of a few parsec, which they interpreted as a transition from three-dimensional to two-dimensional turbulence as one moves from small to large scales. Analytic theory (Goldreich & Sridhar 1995, 1997) and simulations (e.g. Cho, Lazarian & Vishniac 2002; Maron & Goldreich 2001) show that magnetic fields can lead to anisotropic turbulence, which is predicted to exhibit the same power law spectral index as Kolmogorov turbulence. Furthermore, observations of RMs of extragalactic sources (Simonetti & Cordes 1986; Spangler & Reynolds 1990; Clegg et al. 1992) show higher amplitudes of structure in RM in the Galactic plane than out of the plane, suggesting the existence of an addi-

tional source of structure on parsec scales. Results from interstellar scattering show a similar enhancement of structure in the inner Galaxy, but on much smaller scales (Rao & Ananthakrisnan 1984; Dennison et al. 1984; Anantharamaiah & Narayan 1988).

Structure in the ionized ISM can be studied by way of structure functions (SFs). Earlier determinations of SFs of RM using extragalactic sources or the diffuse synchrotron background yielded results that varied widely with scale and area in the sky. Flat structure functions (indicating no structure on the probed scales) found by Simonetti, Cordes & Spangler (1984) on scales larger than 4° towards the Galactic pole were interpreted as showing structure intrinsic to the extragalactic sources with a negligible Galactic contribution. However, this cannot explain the flat SFs from low-latitude extragalactic sources found by Simonetti et al. (1984) on scales $\gtrsim 4^\circ$ and by Clegg et al. (1992) on scales $\gtrsim 1^\circ$. Furthermore, Sun & Han (2004) have recently found shallow SFs of RM in the Galactic plane, and a flat SF at the North Galactic Pole, also from extragalactic sources. Haverkorn, Katgert & de Bruyn (2003a) studied the structure function of RM from diffuse radio emission, and found very shallow slopes for two fields at intermediate latitudes.

In this paper we study the turbulent structure in ionized gas in the inner Galactic plane, by means of SFs of RM from the diffuse synchrotron background, and of SFs of EM from H α emission, both in a region in the inner Galactic plane.

In Section 2 we present our radio polarimetric observations of the Galactic synchrotron background in the Galactic plane. Section 3 discusses the computation of the structure function, while in Section 4 we interpret the structure function as arising from Faraday screens in two spiral arms along the line of sight, both exhibiting turbulent structure. In Section 5, we discuss evidence for enhanced density fluctuations in the Galactic plane, and propose that the structure is dominated by discrete H II regions.

2. THE SOUTHERN GALACTIC PLANE SURVEY TEST REGION

The Southern Galactic Plane Survey (SGPS) is a radio survey in H I and linearly polarized con-

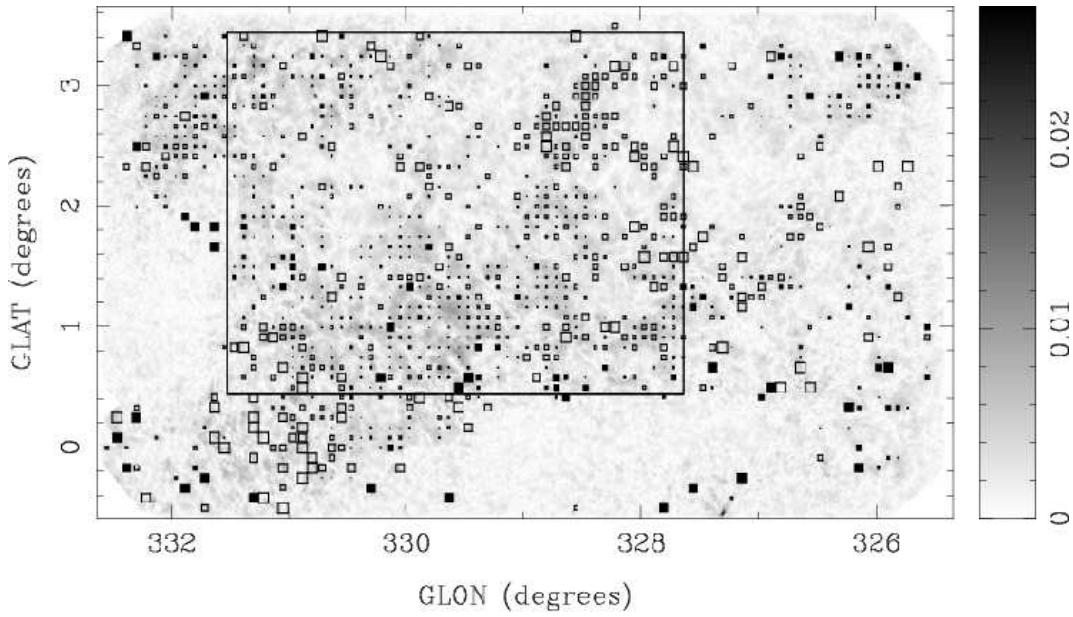


Fig. 1.— Rotation measure in the SGPS Test Region in squares, overlaid on polarized intensity in grey scale given in Jy/beam. Open squares denote negative RMs and filled squares positive ones. The length of a square is proportional to the magnitude of the RM for $|\text{RM}| < 100 \text{ rad m}^{-2}$, and constant for $|\text{RM}| \geq 100 \text{ rad m}^{-2}$. RM values have been given only if $\text{S/N} > 5$ and reduced $\chi^2_r < 2$. The rectangular box drawn in the figure shows the area over which structure functions are computed.

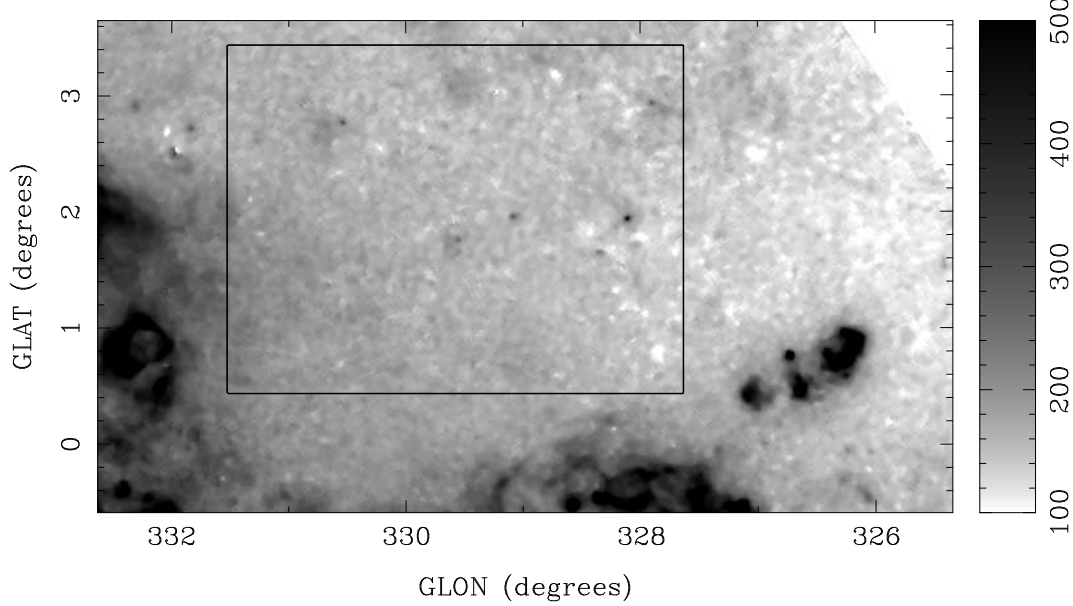


Fig. 2.— H α emission in the SGPS Test Region, from the Southern H-Alpha Sky Survey Atlas (Gaustad et al. 2001). The scale is in deciRayleighs (1 Rayleigh = $10^6/4\pi$ photons $\text{cm}^{-2} \text{s}^{-1} \text{sr}^{-1}$) and the drawn box is the same as in Figure 1. A gradient in emission is visible from the bottom left corner to the top right corner of the box.

tinuum at 1.4 GHz performed with the Australia Telescope Compact Array (ATCA) and Parkes 64m dish (McClure-Griffiths et al. 2001; Gaensler et al. 2001). The first phase of the survey extends over $253^\circ < l < 358^\circ$ and $|b| < 1.5^\circ$, has a spatial resolution of $1'$ and a velocity resolution of 1 km s^{-1} . Before embarking on the complete survey, a Test Region was observed, spanning $325.5^\circ < l < 332.5^\circ$ and $-0.5^\circ < b < 3.5^\circ$ (Gaensler et al. 2001). The continuum data for the SGPS Test Region consists of nine frequency bands each of 8 MHz in width, in the range 1336 MHz to 1424 MHz. From the linear polarization position angle ϕ at these nine frequencies, RMs were derived as $\phi \propto \text{RM} \lambda^2$, where $\text{RM} = 0.81 \int n_e B_{\parallel} ds$ with n_e the thermal electron density in cm^{-3} , B_{\parallel} the component of the magnetic field parallel to the line of sight in μG , and ds the path length in parsecs. Gaensler et al. (2001) give a detailed analysis of the structure in linear polarization and RM in the Test Region, focused on morphology and individual sources. RM fluctuations were apparent in their Figure 7, but not analyzed. We use their data, but use a slightly different algorithm to derive RMs.

Gaensler et al. use a standard algorithm within the data reduction package MIRIAD¹ (Sault & Killeen 2003) to compute RMs, which they describe in detail. The MIRIAD algorithm solves the problem of $n\pi$ radians ambiguity in the polarization angle by first computing an RM value from the first two frequencies. Then, the polarization angles of the other frequencies are rotated $n\pi$ radians so that they lie closest to the angle predicted from the first two frequencies, and the RM is recomputed using these angles. Therefore, a large error in (one of) the two first frequencies can yield the wrong determination of RM. In this way, a small part ($\sim 6\%$) of the RM values Gaensler et al. computed was probably incorrect. Note that all these erratically determined RMs had high reduced χ^2 of the relation $\phi = \text{RM} \lambda^2$, which caused them to be disregarded in their analysis. Therefore the use of this algorithm did not lead to wrong quoted values of RM, but rather to a small number of unjustly disregarded RMs.

Here, we incorporate the ambiguity of polarization angle ϕ by always taking the least pos-

¹<http://www.atnf.csiro.au/computing/software/miriad>

sible angle difference between ϕ in adjacent frequency bands, i.e. $|\phi_i - \phi_j| < \pi$ rad where i and j are adjacent frequencies (Havercorn, Katgert & de Bruyn 2003b; Brown, Taylor & Jackel 2003). The frequencies are so closely spaced that this method renders the correct RM for all $\text{RM} \lesssim 1900 \text{ rad m}^{-2}$. Since in our field RMs are not higher than a few hundred rad m^{-2} and mostly much lower, this is the case for all derived RMs.

Figure 1 shows the RM in the Test Region, superimposed on the continuum polarized intensity in grey scale. The resolution is about $1'$ and the data are about three times oversampled. Open (filled) squares represent negative (positive) RM, and the size of a square is proportional to the magnitude of RM for $|\text{RM}| < 100 \text{ rad m}^{-2}$ and constant for $|\text{RM}| \geq 100 \text{ rad m}^{-2}$. Only every third beam is plotted for clarity. Furthermore, only “reliably determined” RMs are shown, i.e. RMs for which the signal to noise ratio $\text{S/N} > 5$ and the reduced χ^2 of the linear $\phi(\lambda^2)$ fit was $\chi_r^2 < 2$. The dependence of ϕ on λ^2 can be non-linear due to depolarization effects (Burn 1966; Sokoloff et al. 1998). Mild non-linearity is allowed by including reduced χ_r^2 up to 2. About 41% of the data have low enough reduced χ_r^2 , of which 37% has a high enough S/N. So about 15% of the data has reliably determined RMs.

As these data are taken solely with the ATCA interferometer, they lack large-scale information ($\gtrsim 30'$) in the observed Stokes Q and U maps. If a large component of Q and U is missing, the computed values of polarization angle will be incorrect, and therefore the RM will be in error as well. However, the polarization angle depends very non-linearly on Q and U , so that a large missing component in Q and/or U would destroy the linear relation between ϕ and λ^2 . The fact that so many RM’s with low reduced χ^2 are observed suggests that any missing large-scale components should be small. This needs to be confirmed with data from the single dish Parkes telescope, which will be the subject of future studies.

We note that the inability to detect large-scale structure in Stokes Q and U images due to the lack of single-dish data *does not* imply an inability to detect large-scale components in RM. As long as small-scale structure in RM exists superimposed on any large-scale RM, the complete Q and U signals will be detected, which correspondingly allow

us to retrieve the *total* RM, not just the small-scale component. Therefore, fluctuations in RM can be probed at much larger scales than the maximum spatial scale probed by the interferometer.

As RM only provides information on the product $n_e B_{\parallel}$ integrated over the path length, independent information on the path length integrated distribution of thermal electrons is extremely useful for estimation of the structure in the magnetic field. Therefore, we also used emission measure EM = $\int n_e^2 ds$ data from the Southern H-Alpha Sky Survey Atlas (SHASSA, Gaustad et al. 2001), which provides comparable resolution H α data of the Southern sky, see Figure 2. Caution is needed in comparing RM and EM, as the path lengths may not be the same, and the H α data is not corrected for dust extinction. The SHASSA provides data which is median filtered over four 0.8' pixels to remove star residuals, and has a sensitivity of about 0.5 Rayleigh (1 R = $10^6/4\pi$ photons cm $^{-2}$ s $^{-1}$ sr $^{-1}$, corresponding to EM ≈ 2 cm $^{-6}$ pc at T = 8000 K).

3. DETERMINATION OF STRUCTURE FUNCTIONS

Ideally, the scales of variability in a signal such as RM are determined by the power spectrum. However, as the RM data contain blank spaces in the regular grid, we use structure functions (SFs) instead (Simonetti et al. 1984; Minter & Spangler 1996). We define the second order structure function SF of RM and EM as a function of distance lag \mathbf{r} as

$$SF_{RM}(\mathbf{r}) = \langle (RM(\mathbf{x}) - RM(\mathbf{x} + \mathbf{r}))^2 \rangle_{\mathbf{x}} \quad (1)$$

$$SF_{EM}(\mathbf{r}) = \langle (EM(\mathbf{x}) - EM(\mathbf{x} + \mathbf{r}))^2 \rangle_{\mathbf{x}} \quad (2)$$

where $\langle \rangle_{\mathbf{x}}$ denotes the averaging over all positions \mathbf{x} in the field.

Structure functions of RM and EM were determined in the area of the SGPS Test Region for which the most data were available, i.e. within the box drawn in Figs. 1 and 2. The noise was taken into account by subtracting a SF of the error δ in the RM data from SF_{RM}, as explained in the Appendix. We computed one-dimensional SFs for different position angles α (positive b through positive l) of the distance lag vector \mathbf{r} , with an interval of $\Delta\alpha = 10^\circ$.

The left hand plots in Figure 3 give the SFs of RM (top) and EM (bottom) for different position angles $0^\circ < \alpha < 180^\circ$ superimposed for regular sampling in r . Errors in the SF are typically $\log(SF_{RM}) \lesssim 0.05$. The two SFs agree remarkably well: both are very shallow; the slope of SF_{RM} is ~ 0.2 and the slope of SF_{EM} ~ 0.25 for $4' \lesssim r \lesssim 5'$. The slope of SF_{RM} shows a break, below which the SF steepens to ~ 0.5 . Furthermore, at larger scales an anisotropy occurs with position angle in both SFs. A linear fit to the slope at large scales was performed for each position angle over the range given by the horizontal lines in the left hand plots. The slopes of these linear fits are given in the right hand plots of Figure 3. The anisotropy on large scales in the SFs of both RM and EM is more or less sinusoidal, with a maximum for RM and EM at the same position angle $\alpha \approx -50^\circ$.

The sudden change in slope on scales smaller than the break is probably not due to resolution effects in the RM data, as the resolution of the RM data is FWHM = 86'' ($\log(r) \approx -1.6$), which is well below the break. In the EM data, a median filtering over 4 pixels means that at scales $\log(r) > -1.17$, beams are independent, so that the position of the break in SF_{RM} falls below the resolution of the H α data. The unsmoothed data (with a resolution of 0.8') are too contaminated with point sources to determine if a break in the spectrum is present in those data.

The anisotropy in the SF slope at large scales is not an artifact of the gridding or the coordinate system, as its maximum does not coincide with one of the axes. Furthermore, we constructed one-dimensional SF's of the same data in (RA, dec) coordinates. The slopes of these SF's show maxima at the same intrinsic position angle as the data in Galactic coordinates, confirming that the anisotropy is not an artifact of the gridding of the data. The same analysis has also been applied to maps of the Stokes Q and U parameters, and to a map of randomly scrambled RM values in which the observed RMs are redistributed at random positions in the field. The SF's of none of these maps showed an anisotropy, again indicating that the change in slope of SF with direction is physical and not an artifact.

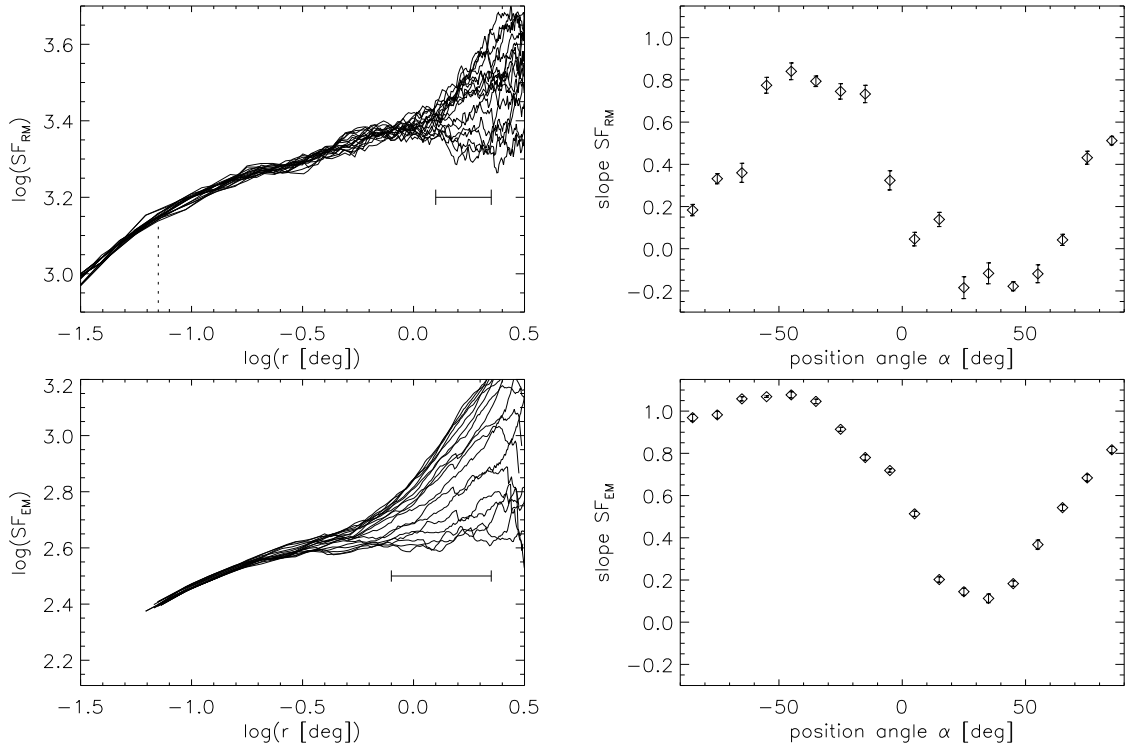


Fig. 3.— Top left: Structure functions of RM, SF_{RM} , in the SGPS Test Region for different position angles $0^\circ < \alpha < 180^\circ$ (positive b through positive l) superimposed. The vertical dotted line shows the position of the break in slope, and the horizontal line gives the range over which the linear fit was performed to yield the slope given in the right hand plot. Top right: dependence of the slope of SF_{RM} on position angle α . Bottom: The same for SF_{EM} .

4. INTERPRETATION OF THE STRUCTURE FUNCTIONS

4.1. The Anisotropy of the SF Slope at Large Scales

Two very different characteristics of a medium can produce an anisotropy of the slopes of SFs: anisotropic turbulence and a large-scale gradient in the medium.

If a strong enough large-scale magnetic field is present in the turbulent ionized medium, the turbulence will be anisotropic (e.g. Goldreich & Sridhar 1995, 1997; Cho & Vishniac 2000). Observing anisotropic turbulence through RM data is believed to be difficult or even impossible because the anisotropy is directed with respect to the *local* magnetic field (Cho et al. 2002), so that structure in the magnetic field along the line of sight is likely to destroy any observational effects of the anisotropic turbulence. If anisotropic turbulence is present in the SFs, it should be seen on all scales instead of only large ones. Furthermore, anisotropic turbulence would yield a set of SFs as a function of position angle which have the same amplitude of fluctuations but on different scales. This is not the case in our observations, where slopes vary from ~ 1 to below zero with position angle. Therefore, we do not believe that the anisotropy in the slope of the SF is caused by anisotropic turbulence.

If the anisotropy in the slope is caused by a gradient across the field, one would expect a steep SF slope in the direction of the gradient, and a flat SF slope in the perpendicular direction. Noise and the superposition of a regular structure like a sinusoid can decrease the slope to below zero. This variation in slope to values below zero is exactly what we observe in both SF_{RM} and SF_{EM} . In fact, in the $H\alpha$ data the gradient can be directly seen in the maps (Figure 2). An $H\alpha$ map of a larger region shows a complex of H II regions and supernova remnants extending over more than 15 degrees in Galactic longitude at higher longitude and lower latitude from the SGPS Test Region, and the EM from that complex decreasing towards and across the Test Region. This coincides with the direction of the gradient computed from the SFs.

A maximum amount of fluctuations in RM at

the position angle -50° does not determine if the gradient is directed towards -50° or 130° . To find the direction of the RM gradient, we looked at the correlation between the magnitude of EM and RM. Figure 4 shows the average EM in bins of $|RM|$ with width $\Delta RM = 10 \text{ rad m}^{-2}$. The magnitudes of EM and RM are clearly correlated, indicating that the gradient in $|RM|$ follows the gradient in EM. Therefore $|RM|$, like EM, decreases towards $\alpha = -50^\circ$. This is to be expected if gradients in electron density and/or path length dominate, and the magnetic field either shows the same gradient or does not change significantly over the field.

To determine what kind of gradient could produce an anisotropy in the slope of SF as observed, we modeled the anisotropy in SF_{RM} using three simple functions: a linear gradient, a broad sinusoid and a Gaussian decrease, all with the gradient oriented at $\alpha = -50^\circ$. Figure 5 shows the results of the modeling with each of these three functions, compared to the data given by the diamonds. The linear gradient is given by the dotted line, the sinusoid by the dashed line, and the Gaussian is denoted by the dash-dotted curve. Noise is included in the models at $RM_{noise} = 5 \text{ rad m}^{-2}$, similar to the noise level in the data. These simplified models show an anisotropy in the slope of comparable amplitude and minimum to the data, although we cannot distinguish between them. More elaborate modeling of the anisotropy in the SF slope is beyond the scope of this paper.

The three models fit best for a total gradient in RM across the field of $\Delta RM \approx 3 \text{ rad m}^{-2}$, while the $H\alpha$ data show a change in EM of about $10 \text{ cm}^{-6} \text{ pc}$ (~ 5 Rayleigh at $T \approx 8000 \text{ K}$). These changes can be due to gradients in electron density or the path length, and most likely a combination of these, possibly accompanied by a gradient in magnetic field. Therefore the measured ΔRM and ΔEM give too few constraints to estimate the gradients separately in magnetic field strength and electron density.

4.2. The Shallow Slope and Break

A structure function of RM produced by a slab of Kolmogorov turbulence with an inner scale r_i and an outer scale r_o is shown as the solid line in the upper panel of Figure 6 (e.g. Stinebring & Condon 1990). The SF is constant on small

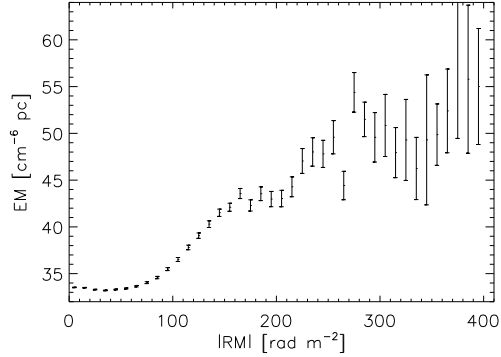


Fig. 4.— Average EM in bins of absolute RM with width $\Delta|\text{RM}| = 10 \text{ rad m}^{-2}$. The errors are the errors in the mean within a bin.

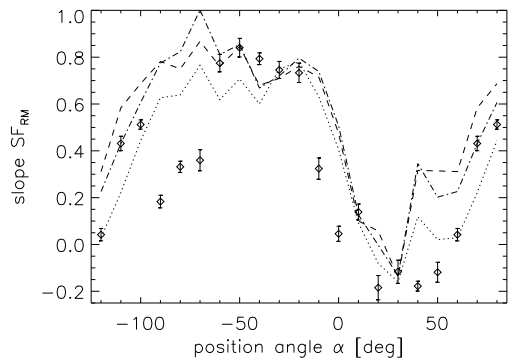


Fig. 5.— Slope of SF_{RM} as a function of position angle α (diamonds), and models of a linear gradient (dotted), a broad sinusoid (dashed), and a Gaussian (dash-dotted). A noise component of 5 rad m^{-2} has been added to the model RMs, comparable to the noise in the data.

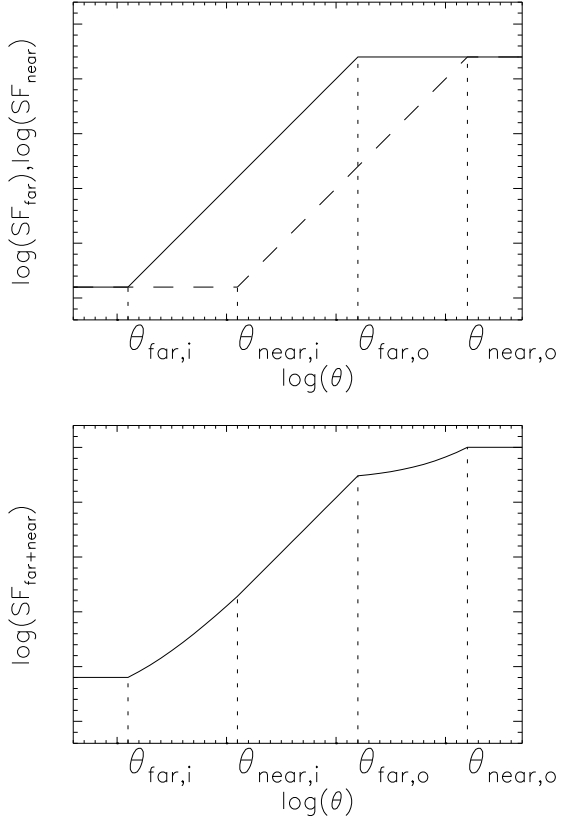


Fig. 6.— Example of the superposition of two Kolmogorov-like structure functions. Top: two structure functions of turbulent Faraday screens with an outer scale r_o and an inner scale r_i , at distances “near” (dashed) and “far” (solid). Bottom: the addition of the two structure functions in the top panel shows a break in the slope, with a shallower slope at large scales.

scales due to dissipation at the inner scale, and then starts to rise at r_i . If the spatial fluctuation in RM is a statistically homogeneous and isotropic random variable and the spectrum of RM is a power law with spectral index s , the slope of the SF b ($SF_{RM} \propto r^b$ for $r_i < r < r_o$) is related to s as (Simonetti et al. 1984):

$$SF_{RM}(r) \propto r^b \text{ where } b = \begin{cases} s-2 & 2 < s < 4 \\ 2 & s > 4 \end{cases} \quad (3)$$

Therefore a Kolmogorov spectrum ($s = 11/3$) should exhibit a structure function slope $b = 5/3$. Above the outer scale of structure r_o , the structure function saturates to the constant value of $2\sigma_{RM}^2$, where σ_{RM}^2 is the variance of the RM distribution.

However, the observed SFs do not show this behavior. In the observed SF_{RM} , a break is visible, and the slope at scales larger than the break is very shallow. This behavior can be most easily explained by the superposition of two Faraday screens at different distances, both with a Kolmogorov-like SF and with certain physical inner and outer scales. Even if the *physical* scales of the structure in these screens are equal, the RM will exhibit structure on different *angular* scales, as shown in Figure 6. The upper panel shows two Kolmogorov-like SFs with the same amplitude at different angular scales θ . In the lower panel the sum of the two SFs is shown, revealing both a break and a shallow spectrum, as observed in Figure 3.

Due to a larger electron density and magnetic field strength in the spiral arms (Beck et al. 1996; Frick et al. 2001; Cordes & Lazio 2003), the major contribution to the RM occurs in the spiral arms. Gaensler et al. (2001) determined that the observed polarized emission originates predominantly from the Crux arm at a distance of 3.5 kpc from the Sun. The major contribution to the RM is most likely made by the Carina and Local spiral arms, located at 100 pc and 1.5 kpc from the Sun, respectively. Then, the Local arm corresponds to the nearby screen in Figure 6, and the Carina arm to the far screen. The break in the SF can be interpreted as the location of the outer scale of structure in the far screen, and therefore denotes the outer scale of the fluctuations in the Carina spiral arm with $r_{far,o} \approx 2$ pc. Similarly, a lower limit to the outer scale of fluctuations in the nearby

screen is given by the position at which the large-scale anisotropy starts dominating the spectrum, i.e. $\log(r) = 0$. This corresponds to the outer scale of structure in the Local Arm $r_{near,o} \gtrsim 1.7$ pc. The shallow slope of SF_{EM} confirms this hypothesis, as the H α emission in this direction is believed not to originate farther away than 1 – 2 kpc, so all H α emission from the Crux arm would be absorbed by intervening dust. Note that Enßlin & Vogt (2003) demonstrated that the autocorrelation length of the Galactic magnetic field is smaller than the autocorrelation length of the RM in typical astrophysical situations, so that the given values for the outer scale of structure could be an upper limit.

5. H II REGIONS AS THE DOMINANT SOURCE OF STRUCTURE

The only other comparable study of EM and RM fluctuations is that made by Minter & Spangler (1996). Minter & Spangler found an outer scale for three-dimensional turbulence in ionized gas of around 4 pc in a region of about 100 square degrees centered at $(l, b) = (143^\circ, -21^\circ)$, but concluded that two-dimensional turbulence extended to larger scales of at least several hundred parsecs. Similarly, Simonetti & Cordes (1986) found structure in the RM of extragalactic point sources in a region at $70^\circ < l < 110^\circ$, $-45^\circ < b < 5^\circ$ on scales of 4° up to 40° , equivalent to 35 to 400 pc at a distance of 2 kpc. Studies of velocity fluctuations in neutral gas also provide evidence for turbulence out to scales of 100 – 1000 pc (Larson 1979; Padoan et al. 2001).

These results are all in striking contrast to the structure function analyses presented in Section 3, where we provide evidence that the outer scale for fluctuations in the density of ionized gas is only $r_o = 1\text{--}2$ pc. Because of the ubiquity of the turbulent cascade otherwise seen in ionized gas over at least 12 orders of magnitude in scale (Armstrong et al. 1995), we are reluctant to interpret our result as indicating that a different physical mechanism is operating in our particular region. Rather, we interpret our results as being due to an additional component of turbulence in the warm ISM. We propose that there are two contributions to turbulence in ionized gas: the overall cascade from the very largest Galactic scales described by Arm-

strong et al. (1995) found throughout the ISM; and a more localized source of turbulence with an outer scale of ~ 2 pc, possibly of much stronger amplitude, found only in the Galactic plane.

There is already good evidence to support such a possibility. The previous analyses of fluctuations in $\text{H}\alpha$ emission and in Faraday rotation which have argued for an outer scale $r_o \gtrsim 100 - 1000$ pc, have focused on sources at high Galactic latitudes, in the outer Galaxy, or in specific localized regions. However, studies of turbulence including the ionized gas in the Galactic plane of the inner Galaxy generally show enhanced turbulence in those regions. Clegg et al. (1992) considered RMs of extragalactic sources in the inner Galaxy and at low latitude ($45^\circ < l < 93^\circ$, $|b| < 5^\circ$). Because their background sources provided only sparse and irregular sampling, Clegg et al. were unable to calculate a continuous structure function with a well-defined slope, as we have done here. However, their data provide clear evidence that at scales $\gtrsim 1^\circ$, the amplitude of RM fluctuations at low latitudes is a factor $> 10^3$ stronger than those seen at high latitudes. Clegg et al. concluded that this results from enhanced turbulence at low latitudes, generated by discrete structures in the Galactic plane. Simonetti & Cordes (1986) also argued for an additional contribution to the turbulence in the Galactic plane by comparing RMs of extragalactic sources in and out of the Galactic plane.

A similar conclusion was reached by Spangler & Reynolds (1990), who compared the EMs towards eight extragalactic sources with the sizes of these sources' scattering disks as measured by VLBI. They found that heavily scattered sources were the same sources which also showed enhanced EMs along their sight lines. They concluded that heavily scattered sources are viewed through an additional component of ionized gas, with turbulent properties distinct from those of the diffuse ionized medium through which weakly scattered sources are seen. Spangler & Reynolds suggested that the additional component is individual H II regions in the Galactic plane. Furthermore, studies of interstellar scintillation of pulsar signals and angular broadening of extragalactic radio sources indicate higher electron density fluctuations in the inner Galaxy than in the solar neighborhood (Rao & Ananthakrishnan 1984; Dennison et al. 1984; Cordes, Weisberg & Boriakoff 1985).

Several studies have tried to characterize the nature of this additional component of structure in the inner Galaxy. Cordes et al. (1985) concluded from pulsar scattering measurements that the ionized plasma had both clumped and nearly uniform components. They suggested that the enhanced scattering in the clumped component could be due to ionization fronts associated with H II regions or shocks associated with stellar winds and supernova shells. Three different components have been identified by Pynzar' & Shishov (1999), based on observations of pulsar scintillation timescales, pulse broadening and dispersion measures. They distinguish a component A as the diffuse gas at high latitudes, which is statistically uniform; a clumpy component BI which is distributed uniformly in the spiral arms and may correspond to Strömgren spheres of O7 to B0 stars; and a clumpy component BII which is concentrated in "compact regions" (~ 1.5 kpc) and is associated with known H II regions or supernova remnants. A similar subdivision was made by Ehle & Beck (1993) for the external spiral galaxy NGC 6946. Ehle & Beck created a model explaining Faraday rotation, depolarization and thermal radio emission as observed at various wavelengths from $\lambda 2.8$ cm to $\lambda 20.5$ cm. Their best fit model contains ionized gas in three components: (1) the diffuse ionized gas with low density and high filling factor; (2) the classical giant H II regions with high density and low filling factor; and (3) small (~ 1 pc) low-density H II regions with intermediate filling factor.

Our measurements appear to confirm this earlier work, in that we similarly have identified a region for which the characteristics of electron density fluctuations are distinct from those found at high latitudes and in quiescent regions. While Simonetti & Cordes (1986), Spangler & Reynolds (1990) and Clegg et al. (1992) showed that the *amplitude* of density fluctuations was enhanced on parsec scales in the inner Galaxy, we have demonstrated that the *outer scale* of such fluctuations is also widely different. We note that Spangler & Reynolds suggested that the parameter which differentiates the two types of turbulence is α^3/r_o , where α is the standard deviation of the density fluctuations divided by the rms density, and represents the depth of density modulation due to turbulence. Spangler & Reynolds es-

timated $r_o \approx 180 \alpha^3$ pc for diffuse ionized gas, and $r_o \approx 1.0 \alpha^3$ pc for regions of enhanced scattering. Assuming strong turbulence ($\alpha \approx 1$) for the regions of strong scattering, they found a typical scale of 1 pc, which is very similar to what we observe here. Other indications that an outer scale of structure of a few parsec may exist in the Galactic plane are presented by Havercorn et al. (2003a). They show SFs of RM from the diffuse synchrotron background in two regions in the second quadrant at latitudes of 8° and 16° . Because they determined the RM from observations at 350 MHz, only the nearby medium (~ 500 pc) is probed, i.e. only the thin disk. The SFs computed by Havercorn et al. may exhibit a break at scales of about 2 pc, and are flat on larger scales. Furthermore, the SF_{RM} of extragalactic sources presented by Lazio, Spangler & Cordes (1990) seem to saturate on scales of a few parsec, although they do not mention this feature. Finally, Simonetti & Cordes (1986) discuss RMs from a region in the Galactic plane and show that there is no structure in this region on scales above 4° .

We therefore confirm the supposition made by earlier authors that in the denser and more complicated regions of our Galaxy found at low latitudes, the dominant source of injection for turbulence appears to be relatively small, discrete, sources. The density fluctuations induced by these sources dominate the turbulent cascade generated at much larger scales which is seen at higher latitudes.

What are the sources likely to be injecting such turbulence? Ionized gas in the Galactic plane is dominated by the contributions from individual H II regions from massive stars. While such sources span a very wide range of sizes, depending on the mass and number of the central powering stars and on the ambient density, there is reasonable evidence that the characteristic scale for such sources is 1 – 2 pc, as implied here. The radius of an idealized Strömgren sphere for the late-type B stars which most likely dominate the population of photo-ionizing sources in the Galaxy is indeed a few pc (e.g. Prentice & ter Haar 1969), while measurements of the sizes of extragalactic H II regions show that the distribution indeed peaks at diameters $< 5 – 10$ pc (Hodge, Lee & Kennicutt 1989; Paladini, Davies & DeZotti 2003).

If the observed structure is mainly due to H II regions from B stars, their number should be suffi-

cient to cover the entire field of view. We can estimate the number of B3 to A0 stars per square parsec of the disk from the Present Day Mass Function (PDMF) presented by Miller & Scalo (1979), and the size of their H II regions from Prentice & ter Haar (1969) (who assume a mean density $n = 1 \text{ cm}^{-3}$). Stars more massive than B3 are excluded because of their scarceness, and stars later than A0 because their H II regions are of negligible size. We construct a three-dimensional model of our field of view, placing B3 to A0 stars randomly in the Local and Carina spiral arms according to the PDMF, and no stars anywhere else. We assume a thickness of 160 pc for both arms (twice the scale height) and the Sun positioned at the far side of the Local arm. The resulting distribution of H II regions is shown in Figure 7. The upper plot shows a two-dimensional cut through the model volume, where the x -axis is directed along the line of sight, the observer is located at $(x, y) = (0, 0)$ and the dashed lines give the field of view of the part of the SGPS Test Region used for the structure function calculation. The lower left plot shows the distribution of the sizes of H II regions, and the lower right plot presents how much of the line of sight is occupied by H II regions, for all independent beams in the region. Clearly, the number of H II regions is enough to dominate the amount of structure at every line of sight.

Interestingly, we note that Armstrong et al. (1995) calculated the contribution of the warm ionized ISM to interstellar turbulence, and concluded that spheres of density $n_e \sim 0.2 \text{ cm}^{-3}$ and radius ~ 2 pc could produce fluctuations comparable to those observed. Armstrong et al. suggested that the amplitudes of fluctuations on such scales were consistent with the turbulent cascade seen at both larger and smaller scales. A calculation of whether our data contain evidence for higher amplitude than or comparable fluctuations to those found elsewhere will be the subject of a later paper in this series.

Mac Low & Klessen (2004) argue that the amount of energy input from H II regions is only a few percent of the energy needed to drive the turbulence in diffuse ionized gas. However, the additional component of turbulence that we observed could be almost entirely due to structure within the H II regions themselves, with a negligible contribution from the turbulence in the diffuse

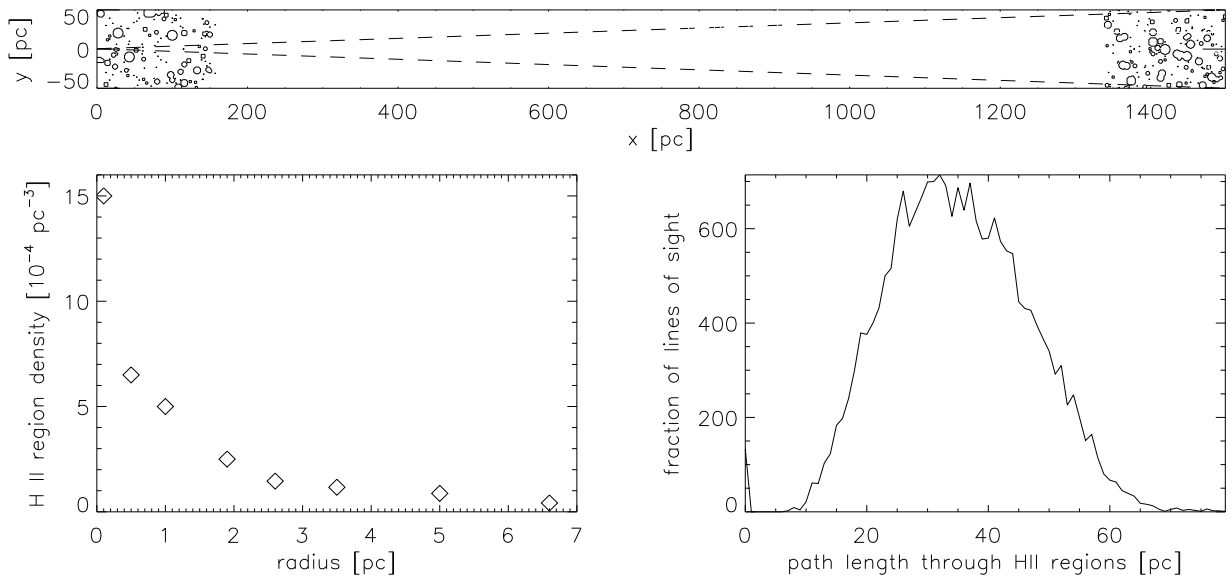


Fig. 7.— Top: two-dimensional cut through a volume distribution of HII regions of B3 to A0 stars. The observer is located at $(x, y) = (0, 0)$, and the dashed lines indicate the field of view of the part of the SGPS Test Region used for the structure function analysis. Stars are randomly positioned in the Local and the Carina spiral arms. The circles indicate the sizes of the individual Strömgren spheres. Bottom: number of HII regions per cubic parsec as a function of their radii (left) and the amount of the line of sight taken up by HII regions for many lines of sight in the field of view (right).

warm ISM (Spangler & Reynolds 1990; Clegg et al. 1992).

If individual H II regions dominate the structure, what is the expected SF spectral index b ? The additional structure component in the ionized gas could be due to discrete edges of H II regions, turbulence inside the H II regions, turbulence in the ISM invoked by the H II regions, or a combination of these. For structure in RM caused only by discrete edges of H II regions SF_{RM} is expected to exhibit a slope $b = 2$ (Rickett, private communication). There is ample observational evidence that H II regions are turbulent (O'Dell 1991; Joncas 1999; Gaensler et al. 2001), but this turbulence may operate on much smaller scales of ~ 0.1 pc (Joncas 1999). The observed steepening of the SF_{RM} slope below $\log(r) \approx -1.1$ possibly constitutes a transition region to steeper slopes of $b = 2$, or to Kolmogorov-like turbulence ($b = 5/3$) on scales $\lesssim 2$ pc.

6. CONCLUSIONS

We have analyzed structure functions (SF) of RM and EM data in the SGPS Test Region. These show very consistent results:

- the SFs of both RM and EM, SF_{RM} and SF_{EM} , exhibit a linear slope in log-log space, with SF_{RM} showing a break at $\sim 4'$ to a flatter slope at larger angular scales;
- the slope at angular scales $\gtrsim 4'$ is shallow though non-zero in both SF_{RM} and SF_{EM} , with a SF spectral index $b \approx 0.2$;
- at scales larger than about a degree, the spectral index of SF_{RM} and SF_{EM} is anisotropic, forming a quasi-sinusoidal dependence on position angle.

The anisotropy in one-dimensional SFs at large scales is explained by a large-scale gradient in electron density, possibly accompanied by magnetic field, across the field of view due to a foreground structure. The break in SF_{RM} and shallowness of the slope in both SF_{RM} and SF_{EM} at smaller scales can be explained by the superposition of two contributions to EM and RM of the Local and Carina spiral arms. Within such a model, we infer the outer scale of structure in the spiral arms to be about 2 pc. As Kolmogorov-like

turbulence is observed in the ISM on scales much larger than a few pc, these results constitute evidence for an additional contribution to turbulent fluctuations in the Galactic plane. The inferred outer scale of fluctuations agrees with the size of Strömgren spheres around the most abundant late-type B stars. Therefore, H II regions could provide the dominant source of structure on pc scales in the Galactic spiral arms.

The suggestion that the break in SF_{RM} and the shallowness of both SF_{RM} and SF_{EM} is due to two separate Faraday screens will be tested in a forthcoming paper by studying SFs in different regions of the sky. This can also shed light on the occurrence of any spatial variations of the turbulent spectrum. Furthermore, the combined RM and EM data should enable at least partial decoupling of magnetic field and electron density, and the amplitudes of the SF will yield information on this additional component of structure in the ionized ISM in the Galactic plane.

We thank Ellen Zweibel, Alex Lazarian, Jungyeon Cho, Dipanjan Mitra and Chris Brunt for stimulating discussions and helpful suggestions. The Australia Telescope is funded by the Commonwealth of Australia for operation as a National Facility managed by CSIRO. The Southern H-Alpha Sky Survey Atlas (SHASSA) is supported by the National Science Foundation. MH and BMG acknowledge the support of the National Science Foundation through grant AST-0307358.

A. NOISE CONTRIBUTION TO THE STRUCTURE FUNCTION

For a rotation measure $\text{RM} \pm \delta \text{ rad m}^{-2}$, the SFs of the RM and the error δ can be separated using

$$\begin{aligned} \text{SF}(\text{RM}_{obs}) &= \langle [(\text{RM}(x) + \delta(x)) - (\text{RM}(x+r) + \delta(x+r))]^2 \rangle \\ &= \langle \text{RM}^2(x) + \text{RM}^2(x+r) - 2\text{RM}(x)\text{RM}(x+r) \rangle + \\ &\quad \langle \delta^2(x) + \delta^2(x+r) - 2\delta(x)\delta(x+r) \rangle \\ &= \text{SF}(\text{RM}) + 2\langle \delta^2 \rangle \tag{A1} \\ &= \text{SF}(\text{RM}) + \text{SF}(\delta) \tag{A2} \end{aligned}$$

since $\langle \text{RM}\delta \rangle = 0$ and $\langle \delta(x)\delta(x+r) \rangle = 0$. Therefore, the contribution of noise in RM (which is assumed Gaussian) can be taken into account by subtracting a SF of a Gaussian distribution of noise with width $\sqrt{\langle \delta^2 \rangle}$ from the SF of the observed RM.

REFERENCES

Anantharamaiah, K. R., & Narayan, R. 1988, in "Radio wave scattering in the interstellar medium", ed. J. M. Cordes, New York, American Institute of Physics, p. 185.

Armstrong, J. W., Rickett, B. J., & Spangler, S. R. 1995, *ApJ*, 443, 209

Beck, R., Brandenburg, A., Moss, D., Shukurov, A., & Sokoloff, D. 1996, *ARA&A*, 34, 155

Brown, J. C., Taylor, A. R., & Jackel, B. J. 2003, *ApJ*, 145, 213

Burn, B. J. 1966, *MNRAS*, 133, 67

Cho, J., Lazarian, A., & Vishniac, E. T. 2002, *ApJ*, 564, 291

Cho, J., & Vishniac, E. T. 2000, *ApJ*, 539, 273

Clegg, A. W., Cordes, J. M., Simonetti, J. M., & Kulkarni, S. R. 1992, *ApJ*, 386, 143

Cordes, J. M., & Lazio, T. J. W. 2003, preprint (astro-ph/0301598)

Cordes, J. M., Weisberg, J. M., & Boriakoff, V. 1985, *ApJ*, 288, 221

Dennison, B., Broderick, J. J., Thomas, M., Booth, R. S., Brown, R. L., & Condon, J. J. 1984, *A&A*, 135, 199

Ehle, M., & Beck, R. 1993, *A&A*, 273, 45

Elmegreen, B. G., Elmegreen, D. M., & Leitner, S. N. 2003, *ApJ*, 590, 271

Enßlin, T. A., & Vogt, C. 2003, *A&A*, 401, 835

Frick, P., Stepanov, R., Shukurov, A., & Sokoloff, D. 2001, *MNRAS*, 325, 649

Gaensler, B. M., Dickey, J. M., McClure-Griffiths, N. M., Green, A. J., Wieringa, M. H., Haynes, R. F. 2001, *ApJ*, 549, 959

Gaustad, J. E., McCullough, P. R., Rosing, W., & Van Buren, D. 2001, *PASP*, 113, 1326

Goldreich, P., & Sridhar, S. 1997, *ApJ*, 485, 680

Goldreich, P., & Sridhar, S. 1995, *ApJ*, 438, 763

Haverkorn, M., Katgert, P., de Bruyn, A. G. 2003a, *A&A*, 403, 1045

Haverkorn, M., Katgert, P., de Bruyn, A. G. 2003b, *A&A*, 403, 1031

Hodge, P., Lee, M. G., & Kennicutt, R. C., Jr. 1989, *PASP*, 101, 32

Joncas, G. 1999, in proceedings of the 2nd Guillermo Haro Conference, Interstellar Turbulence, ed. J. Franco & A. Carraminana, Cambridge University Press, p.154

Kolmogorov, A. N., 1941, *Dokl. Akad. Nauk SSSR*, 30, 301

Korpi, M. J., Brandenburg, A., Shukurov, A., Tuominen, I., & Nordlund, Å 1999, *ApJ*, 514, 99

Larson, S. M. 1979, *MNRAS*, 186, 479

Lazio, T. J., Spangler, S. R., & Cordes, J. M. 1990, *ApJ*, 363, 515

Mac Low, M.-M., & Klessen, R. S. 2004, *Rev. Mod. Phys.*, in press (astro-ph/0301093)

Maron, J., & Goldreich, P. 2001, *ApJ*, 554, 1175

McClure-Griffiths, N. M., Green, A. J., Dickey, J. M., Gaensler, B. M., Haynes, R. F., & Wieringa, M. H. 2001, *ApJ*, 551, 394

Miller, G. E., & Scalo, J. M. 1979, *ApJS*, 41, 513

Minter, A. H., & Spangler, S. R. 1996, *ApJ*, 458, 194

Norman, C. A., & Ferrara, A. 1996, *ApJ*, 467, 280

O'Dell, C. R. 1991, in proceedings of the 147th Symposium of the IAU, ed. E Falgarone, F. Boulanger, & G. Duvert, Kluwer Academic Publishers, Dordrecht, p.476

Padoan, P., Kim, S., Goodman, A., & Staveley-Smith, L. 2001, *ApJ*, 555, 33

Paladini, R., Davies, R. D., & DeZotti, G. 2003, preprint (astro-ph/0309350)

Prentice, A. J. R., & Ter Haar, D. 1969, *MNRAS*, 146, 423

Pynzar', A. V., & Shishov, V. I. 1999, *A. Rep.*, 43, 7, 436

Rao, A. P., & Ananthakrishnan, S. 1984, *Nature*, 312, 707

Sault, R. J., & Killeen, N. E. B. 2003, *The Miriad User's Guide* (Sydney: Australia Telescope National Facility)

Sellwood, J. A., & Balbus, S. A. 1999, *ApJ*, 511, 660

Simonetti, J. H., & Cordes, J. M. 1986, *ApJ*, 310, 160

Simonetti, J. H., Cordes, J. M., & Spangler, S. R. 1984, *ApJ*, 284, 126

Sokoloff, D. D., Bykov, A. A., Shukurov, A., Berkhuijsen, E. M., Beck, R., & Poezd, A. D. 1998, *MNRAS*, 299, 189

Spangler, S. R., & Reynolds, R. J. 1990, *ApJ*, 361, 116

Spitzer, L. 1978, "Physical processes in the interstellar medium", New York Wiley-Interscience

Stinebring, D. R., & Condon, J. J. 1990, *ApJ*, 352, 207

Sun, X. H., & Han, J. L. 2004, in "The Magnetized Interstellar Medium", ed. B. Uyaniker, W. Reich & R. Wielebinski, Copernicus GmbH, in press (astro-ph/0402180)

Vollmer, B., & Beckert, T. 2002, *A&A*, 382, 872